A theoretical study of mean azimuthal flow and asymmetry effects on thermo-acoustic modes in annular combustors

Michaël Bauerheim, Michel Cazalens, Thierry Poinsot

A theoretical study of mean azimuthal flow and asymmetry effects on thermo-acoustic modes in annular combustors

M. Bauerheim [a,b,*], M. Cazalens [c], T. Poinsot [d]

[a] CERFACS, CFD Team, 42 Av Coriolis, 31057 Toulouse, France
[b] Société Nationale d'Etude et de Construction de Moteurs d'Aviation, 77550 Reau, France
[c] Centre de Recherche et Technologies: SAFRAN, France
[d] IMF Toulouse, INP de Toulouse and CNRS, 31400 Toulouse, France

Abstract

The objective of this paper is to develop an analytical model to capture two symmetry breaking effects controlling the frequency and nature (spinning, standing or mixed) of azimuthal modes appearing in annular chambers: (1) Using two different burner types distributed along the chamber (2) Considering the mean azimuthal flow due to the swirlers or to effusion cooling. The ATACAMAC (Analytical Tool to Analyze and Control Azimuthal Modes in Annular Chambers) methodology is applied using the linearized acoustic equations with a steady and uniform azimuthal mean flow. It provides an analytical implicit dispersion relation which can be solved numerically. A fully analytical resolution is possible when the annular chamber is weakly coupled to the burners. Results show that symmetry breaking, either by mixing burners types or with a mean azimuthal flow, splits the azimuthal modes into two waves with different frequencies and structures. Breaking symmetry promotes standing modes but adding even a low azimuthal mean flow fosters spinning modes so that the azimuthal mean flow must be taken into account to study azimuthal modes.

Keywords: Azimuthal; Theoretical; Instabilities; Mean flow; Symmetry

1. Introduction

Thermoacoustic unstable modes are a major problem in combustion systems and they take a specific form in annular chambers. In modern gas turbines, azimuthal modes can develop in a frequency range which coincides with longitudinal modes [1–4]. The nature of these azimuthal modes has been the topic of multiple past studies since the pioneering works of companies like Siemens [1] or Alstom [5] who showed that both spinning or standing azimuthal modes could be observed in an annular gas turbine. Five years ago, the development of powerful LES techniques applied to full annular combustors [6,7] showed that

* Corresponding author at: CERFACS, CFD Team, 42 Av Coriolis, 31057 Toulouse, France. Fax: +33 0 5 61 19 30 00.
E-mail address: bauerheim@cerfacs.fr (M. Bauerheim).

http://dx.doi.org/10.1016/j.proci.2014.05.053

azimuthal modes could change nature randomly, evolving from spinning to standing structure at random instants. Experiments have also been developed [8,9], confirming LES results but also raising additional questions, for example linked to the effect of outlet conditions on the development of modes. Various theories have been proposed [5,10–13], focusing on two questions: (1) what controls the nature and the occurrence of azimuthal modes? and (2) is it possible to suppress them? Most solutions focus on breaking symmetry, for example by mixing burners with different unsteady responses in a given chamber.

A major limitation of both experimental and LES studies in this field is cost. To understand azimuthal modes, simpler tools which allow to explore their basic nature in idealized configurations, are needed. Such tools can be built using network approaches and fully analytical methods [14–16]. Recently, analytical studies have progressed in two directions: (1) Linear theories based on network models [15–17] where the acoustic-flame behavior is assumed linear and modeled by a Flame Transfer Function (FTF) while major features of the configuration are retained such as complex burners, both annular plenum and chamber, mean flow etc. These studies are usually performed to determine the stability of the configuration but can also predict linear effects on mode structure. (2) Non-linear theories based on linearized Galerkin methods [5,13] where the configuration is usually reduced to a simple annulus with zero or an infinite number of burners and no plenum but the acoustic-flame behavior is non-linear and modeled using a Flame Describing Function (FDF). Non-linear approaches are especially designed to study limit cycles and mode structures but they require simplifications. Both linear and non-linear analytical tools, as well as Helmholtz solvers, can only investigate the nature of the two components A and B of the azimuthal modes but fail to estimate their respective amplitudes. Especially, the ratio A/B is ignored and the final structure cannot be fully determined analytically: it requires experiments or high fidelity simulations.

This paper develops a linear approach to investigate two linear mechanisms controlling azimuthal modes by breaking symmetry: (1) Geometrical symmetry (GS) breaking by mixing burners with different responses and (2) Flow symmetry breaking by introducing a mean swirling motion (SM) in the annular chamber. The SM mechanism is shown to play a strong role: it makes the period of the two modes (co-rotating with the mean swirl and counter rotating) different because propagating at $c + w$ or $c - w$ (where w is the swirl velocity and c the sound speed in the chamber). This 'splits' azimuthal modes (which are usually degenerate at zero Mach number) into two distinct modes. This effect is dominant compared to GS breaking and results suggest that the nature of azimuthal modes in annular chambers cannot be analyzed in the zero Mach number limit but must incorporate the effects of a mean azimuthal velocity. All applications are performed for a chamber containing 4 burners but conclusions are expected to be valid for real chambers (N ≃10–30).

2. The analytical model

2.1. Model description

Consider a configuration where N burners feed a 1D annular chamber (Fig. 1). The length and section of the i^{th} burner are noted L_i and S_i while the perimeter and the cross-section of the annular chamber are $2L_c = 2\pi R_c$ and S_c respectively. Points in the burners are located using the axial coordinate z where $z = 0$ designates the upstream end and $z = L_i$ the burner/chamber junction. The i^{th} compact flame location is given by the normalized abscissa $\alpha = z_{f,i}/L_i$. The position in the annular cavity is identified by the angle θ defining the azimuthal coordinate $x = R_c\theta$. An impedance Z is imposed at the upstream end of each burner ($z = 0$).

This model is limited to purely azimuthal modes where acoustic fluctuations in the chamber depend only on the azimuthal coordinate (θ or $x = R_c\theta$): it does not apply to academical setups open to the atmosphere [8,9,18] but corresponds well to real chambers terminated by a choked nozzle ($w' = 0$). Mean density and sound speed are noted ρ^0 and c^0 in the annular chamber and in the hot part of the burners ($\alpha L_i < z < L_i$) and ρ_u^0 and c_u^0 in the cold part of the burners ($0 < z < \alpha L_i$).

Different types of burners are used to study GS breaking (Section 3.4) and a mean azimuthal flow is imposed in the chamber to study SM breaking (Section 3.3). This mean flow field is supposed to be one dimensional, steady and uniform:

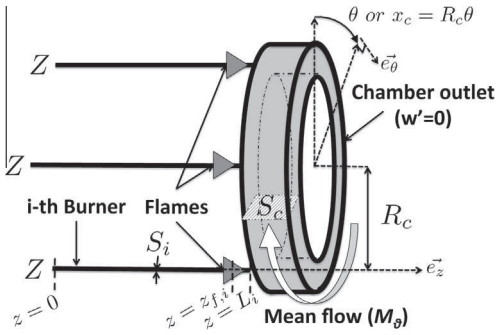

Fig. 1. Configuration to study unstable modes in annular chambers with a steady and uniform azimuthal flow (constant Mach number M_θ).

$$\vec{u_0}(x,t) = u_0(x,t)\vec{e_\theta} = M_\theta c^0 \vec{e_\theta} \quad (1)$$

where $\vec{e_\theta}$ is the azimuthal vector and $M_\theta = u_0/c^0$ is the azimuthal Mach number. Such swirling motions are often observed in annular chambers because all swirlers have the same rotation direction. In many recent chamber designs, where effusion systems are used to introduce additional azimuthal rotation and modify residence times, the azimuthal Mach number can be fairly large (M_θ up to 0.1). Note however that swirl directions induced by swirlers are in opposite directions along the outer and inner annular walls, with a faster azimuthal velocity towards the inner wall and a slower one towards the outer wall due to different path lengths. Here only a mean bulk swirl is considered but [9,19] have shown experimentally that acoustic-combustion interaction may be different in the inner and outer regions of the swirlers.

2.2. ATACAMAC methodology and analytical dispersion relation

The ATACAMAC (Analytical Tool to Analyze and Control Azimuthal Modes in Annular Chambers) [15,17] methodology is used to reduce the size of the system by splitting the annular combustor into N sectors (Fig. 2). Each sector is split into two parts: an azimuthal propagation in the annular chamber and an interaction area at the burner/chamber junction.

2.2.1. Interaction area at the burner/chamber junction

The area where the acoustic interaction between the i^{th} burner and the annular chamber occurs (Fig. 2) is compact [20]. The effect of the i^{th} burner on the acoustic field can be modeled by a translated impedance $Z_{tr}(Z,\alpha,L_i,n_i,\tau_i) = \frac{p'_{b,i}(z=Li)}{\rho^0 c^0 w'_{b,i}(z=L_i)}$ [21].

The linearized equations of conservation of mass and momentum for isentropic ($p' = c^{0^2}\rho'$) configurations with non-zero azimuthal Mach number (Fig. 3) discussed in [22–25] are applied at the T-junction (mean flow is added only in the chamber but no mean flow is introduced in the burners along the longitudinal direction $\vec{z}$, i.e. $M_z = 0$) which contains only burnt gases (Figs. 2 and 3):

$$m'_i + m'_{b,i} = m'_{i+1} \text{ and } D'_i = D'_{i+1} = D'_b \quad (2)$$

where $m' = (\bar{\rho}u' + \rho'\bar{u})S$ is the linearized mass flow rate through the surface S and $D' = p' + 2\bar{\rho}\bar{u}u' + \rho'\bar{u}^2$ is the linearized acoustic momentum where $\bar{f}$ and f' designates the mean and fluctuating quantity of f respectively.

With an azimuthal mean flow in the chamber, these equations become at the T-junction:

$$[p'_{i+1} - p'_{i+\frac{1}{2}}]M_\theta S_c = \rho^0 c^0 [u'_{i+\frac{1}{2}} S_c + w'_{b,i}(z=L_i)S_i - u'_{i+1}S_c] \quad (3)$$

$$p'_{i+\frac{1}{2}}(1+M_\theta^2) + 2\rho^0 c^0 M_\theta u'_{i+\frac{1}{2}} = p'_{b,i}(z=L_i) = p'_{i+1}(1+M_\theta^2) + 2\rho^0 c^0 M_\theta u'_{i+1} \quad (4)$$

or in matrix form:

$$\begin{bmatrix} p' \\ -j\rho^0 c^0 u' \end{bmatrix}_{i+1} = T_i \begin{bmatrix} p' \\ -j\rho^0 c^0 u' \end{bmatrix}_{i+\frac{1}{2}} \quad (5)$$

where the interaction matrix T_i is:

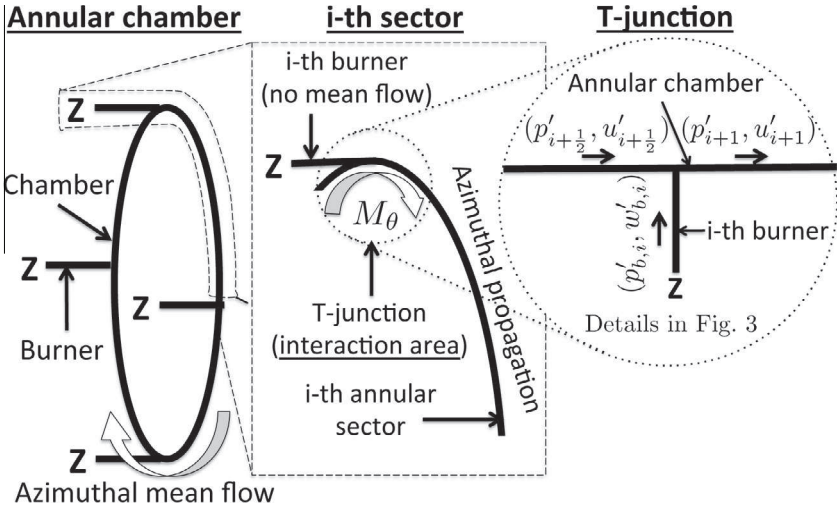

Fig. 2. Configuration with $N = 4$ burners (left) and zoom on i^{th} sector (middle) and i^{th} T-junction (right).

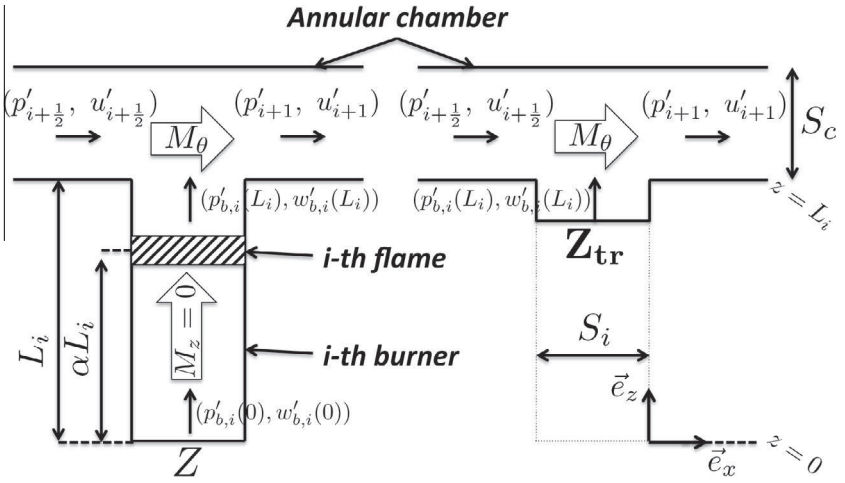

Fig. 3. Equivalent impedance of the i^{th} burner: the translated impedance Z_{tr} takes into account the upstream impedance Z, the propagation in the cold ($0 < z < \alpha L_i$) and hot ($\alpha L_i < z < L_i$) parts of the burner as well as the active flame (at $z = \alpha L_i$).

$$T_i = I_d + \mathcal{G}_i \begin{bmatrix} -4j\frac{M_\theta}{1+M_\theta^2} & 8\left(\frac{M_\theta}{1+M_\theta^2}\right)^2 \\ 2 & 4j\frac{M_\theta}{1+M_\theta^2} \end{bmatrix} \tag{6}$$

where $\mathcal{G}_i = \frac{(1+M_\theta^2)^2}{1-M_\theta^2}\Gamma_i$ is the coupling parameter at non-null Mach number and $j = \sqrt{-1}$. It is related to the coupling parameter without mean flow Γ_i [15,17,26,27] linked to the equivalent impedance Z_{tr} of the i^{th} burner (Fig. 3):

$$\Gamma_i = S_c/(2jS_iZ_{tr}) \tag{7}$$

2.2.2. Propagation in the i^{th} annular sector

Pressure and velocity fluctuations can be written at any location x in the annular chamber as [15,28]:

$$\begin{cases} p'_x & (Ae^{jk^+x} + Be^{-jk^-x})e^{-j\omega t} \\ \rho^0 c^0 u'_x & (Ae^{jk^+x} - Be^{-jk^-x})e^{-j\omega t} \end{cases} \tag{8}$$

where $k^\pm = \frac{\omega/c^0}{1\pm M_\theta}$.

Eq. (8) yields:

$$\begin{bmatrix} p' \\ -j\rho^0 c^0 u' \end{bmatrix}_{x+\Delta x} = R(\Delta x) \begin{bmatrix} p' \\ -j\rho^0 c^0 u' \end{bmatrix}_x \tag{9}$$

where the propagation matrix $R(\Delta x)$ is:

$$R(\Delta x) = \frac{e^{jk^+\Delta x}}{2}\begin{bmatrix} 1 & j \\ -j & 1 \end{bmatrix} + \frac{e^{-jk^-\Delta x}}{2}\begin{bmatrix} 1 & -j \\ j & 1 \end{bmatrix} \tag{10}$$

Knowing that for each sector the azimuthal propagation distance is the same ($\Delta x = 2L_c/N$), all propagation matrices are equal and written $R(2L_c/N)$.

2.2.3. Analytical dispersion relation

Since interaction (Eq. (5)) and propagation (Eq. (10)) matrices are known, the transfer matrix M_i of the i^{th} sector can be obtained:

$$\begin{bmatrix} p' \\ -j\rho^0 c^0 u' \end{bmatrix}_{i+1} = \underbrace{[T_i].[R(2L_c/N)]}_{M_i} \begin{bmatrix} p' \\ -j\rho^0 c^0 u' \end{bmatrix}_i \tag{11}$$

Finally, the periodicity of the system and the equation of one sector (Eq. (11)) lead to:

$$\begin{bmatrix} p' \\ -j\rho^0 c^0 u' \end{bmatrix}_N = \left(\prod_{i=N}^{1} M_i\right) \begin{bmatrix} p' \\ -j\rho^0 c^0 u' \end{bmatrix}_N \tag{12}$$

The system (12) has non trivial solutions only if its determinant is null leading to an implicit analytical dispersion relation for the frequency f:

$$det\left(\prod_{i=N}^{1} M_i - I_d\right) = 0 \tag{13}$$

where I_d is the 2-by-2 identity matrix.

2.3. Analytical resolution for a chamber with $N = 4$ burners

The implicit dispersion relation (Eq. (13)) can be solved analytically using an asymptotic approach for low coupling factor Γ_i or $\mathcal{G}_i$:

$$\forall i \in [1, N], \|\mathcal{G}_i\| \ll 1 \tag{14}$$

The matrix $M = \prod_{i=4}^{1} M_i = M_2M_1M_2M_1$ corresponds to the asymmetry pattern 1212 and to the symmetric configuration if $M_1 = M_2$ is enforced ($\Gamma_1 = \Gamma_2$). The Taylor expansion of this matrix (called $\widetilde{M}$) around the frequency of the

annular rig alone ($f = f^0 + \delta f$ [15,17] where $f^0 = c^0/2L_c$ for the first azimuthal mode) at first order assuming low coupling factors (Eq. (14)) and low Mach number $M_\theta \ll 1$ is:

$$\widetilde{\prod_{i=4}^{1} M_i} = I_d + 2\pi \begin{bmatrix} -jM_\theta & -\frac{2L_c}{c^0}\delta f - \frac{2}{\pi}\mathcal{G}_1^{0,\pm M_\theta} \\ \frac{2L_c}{c^0}\delta f + \frac{2}{\pi}\mathcal{G}_2^{0,\pm M_\theta} & -jM_\theta \end{bmatrix} \tag{15}$$

where $\mathcal{G}_1^{0,\pm M_\theta}$ and $\mathcal{G}_2^{0,\pm M_\theta}$ are the values of the coupling parameters $\mathcal{G}_1$ and $\mathcal{G}_2$ evaluated at the frequency $f^0(1 \pm M_\theta)$.

Eq. (15) yields an explicit dispersion relation:

$$\left(2\pi\frac{L_c}{c^0}\delta f\right)^2 + 4\pi\frac{L_c}{c^0}\left(\mathcal{G}_1^{0,\pm M_\theta} + \mathcal{G}_2^{0,\pm M_\theta}\right)\delta f + 4\mathcal{G}_1^{0,\pm M_\theta}\mathcal{G}_2^{0,\pm M_\theta} - \pi^2 M_\theta^2 = 0 \tag{16}$$

Frequencies of the first azimuthal mode can be obtained by solving the quadratic equation (Eq. (16)). They are recast using nondimensionalized numbers such as the mean azimuthal Mach number, the total coupling factor ($\Sigma_0 = 2(\mathcal{G}_1^{0,\pm M_\theta} + \mathcal{G}_2^{0,\pm M_\theta})$) and the splitting strength ($\mathcal{S}$) defined for the pattern 1212 as:

$$\mathcal{S} = 2(\mathcal{G}_1^{0,\pm M_\theta} - \mathcal{G}_2^{0,\pm M_\theta}) \tag{17}$$

so that solutions of Eq. (16) are:

$$\delta f_{1,2} = -c^0\left(\Sigma_0 \pm \sqrt{\mathcal{S}^2 + 4\pi^2 M_\theta^2}\right)/4\pi L_c \tag{18}$$

where $-$ corresponds to Wave 1 (co-rotating if $M_\theta \neq 0$) and $+$ to Wave 2 (counter-rotating if $M_\theta \neq 0$): the frequencies are split.

The eigenspace associated to each frequency ($f_1 = f^0 + \delta f_1$ and $f_2 = f^0 + \delta f_2$) is one-dimensional and the mode nature is fixed by M_θ and $\|\mathcal{S}\|$. The system defined by Eq. (12) can be evaluated at the frequencies f_1 and f_2 obtained in Eq. (18) which provides the relation:

$$\begin{bmatrix} -2\pi jM_\theta & -\mathcal{S} \pm \mathcal{S}_M \\ -\mathcal{S} \mp \mathcal{S}_M & -2\pi jM_\theta \end{bmatrix} \begin{bmatrix} p' \\ -j\rho^0 c^0 u' \end{bmatrix}_4 = \begin{bmatrix} 0 \\ 0 \end{bmatrix} \tag{19}$$

where $\mathcal{S}_M = \sqrt{\mathcal{S}^2 + 4\pi^2 M_\theta^2}$ corresponds to the interaction of GS ($\mathcal{S}$) and SM (M_θ) breaking.

For Waves 1 and 2, Eq. (19) gives the ratio $\frac{q^+}{q^-} = \frac{p'_4 + \rho^0 c^0 u'_4}{p'_4 - \rho^0 c^0 u'_4}$:

$$\frac{q^+}{q^-} = \frac{-\mathcal{S}}{2\pi M_\theta + \mathcal{S}_M} \text{ and } \frac{q^+}{q^-} = \frac{2\pi M_\theta + \mathcal{S}_M}{\mathcal{S}} \tag{20}$$

Consequently the frequency and nature of azimuthal modes are controlled by the splitting strength $\|\mathcal{S}\|$, the Mach number M_θ and their interaction $\|\mathcal{S}_M\|$.

3. Results and discussion

3.1. Description of the configurations

The effect of geometrical and flow symmetry breaking on frequency and nature of azimuthal modes will be investigated using the analytical results (Eqs. (18) and (20)) in an idealized annular combustor with $N = 4$ burners (Fig. 4). Only the first azimuthal mode is considered. Physical and geometrical parameters are defined in Table 1 and Fig. 4. The upstream impedance Z is set to zero to mimic a large plenum connected to the burners and the flames are placed at the burner/chamber junction ($\alpha = 1$) which leads to [17]:

$$\Gamma_i = -\frac{1}{2}\frac{S_i}{S_c}\frac{\rho^0 c^0}{\rho_u^0 c_u^0}(1 + n_i e^{j\omega\tau_i})\,\text{cotan}\,(k_u L_i) \tag{21}$$

where $k_u = \omega/c_u$.

Four different cases (Fig. 5) are studied:

- **Sym-NoMach:** First, a symmetric configuration where burners and flames are identical is studied (Section 3.2, [15]. The Mach number M_θ is zero.
- **Sym-Mach:** A constant mean azimuthal flow ($M_\theta \neq 0$) is added to the previous case.
- **Asym-NoMach:** At zero Mach number ($M_\theta = 0$), the configuration is disymmetrized using two burner types with different Flame Transfer Functions (n_1, τ_1) and (n_2, τ_2) with the pattern 1212 (Section 3.4).
- **Asym-Mach:** Finally, an azimuthal mean flow corresponding to a mean Mach number M_θ is added to the previous case (Section 3.5).

Analytical results are systematically compared to numerical solutions of the eigen-problem (12): the frequencies are computed using a non-linear solver (Newton–Raphson) searching for zeros of $det(\prod_{i=N}^{1} M_i - I_d)$.

Knowing the frequency, the state at the N^{th} burner location ($V_N = (p'_N, -j\rho^0 c^0 u'_N)^T$) is computed as an eigenvector satisfying Eq. (12). The acoustic pressure p'_N and velocity u'_N are propagated at any azimuthal location x in the chamber using Eqs. (5) and (10). The azimuthal variation of the pressure modulus ($\|p'\|$) and phase ($\phi = \arg(p')$) with the azimuthal coordinate (x or θ) indicates the mode nature: spinning (linear phase), standing (constant phase) or mixed. A structure diagram ($\|p'\|\cos(\phi), \|p'\|\sin(\phi), M_\theta$ or $\|\mathcal{S}\|$) is constructed to track the evolution of the mode structure with the Mach number (M_θ) or the splitting strength ($\|\mathcal{S}\|$).

Analytical results with no mean flow will be also validated using a 3D acoustic solver called AVSP devoted to the resolution of acoustic modes at zero Mach number of combustion chambers [29].

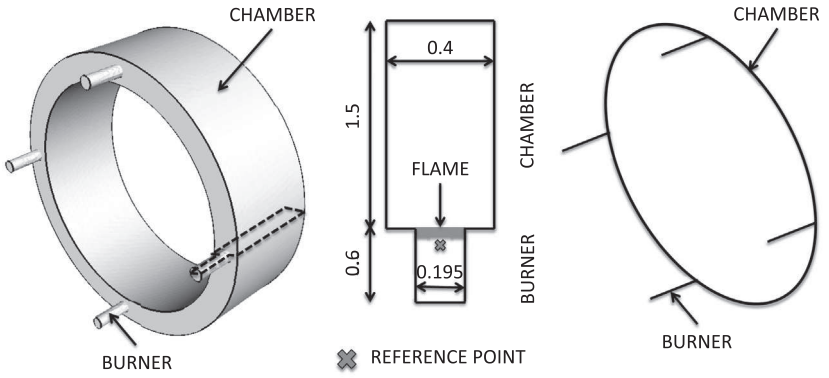

(a) 3D view of the BC configuration (b) Axial cut (c) 1D model for ATACAMAC

Fig. 4. Configuration with $N = 4$ burners.

Table 1
Parameters used for numerical applications corresponding to a large scale industrial gas turbine.

Chamber	L_c	6.59	m
	S_c	0.6	m^2
Burner	L_i^0	0.6	m
	S_i	0.01	m^2
Fresh gases	ρ_u^0	9.79	kg/m^3
	c_u^0	743	m/s
Burnt gases	ρ^0	3.81	kg/m^3
	c^0	1191	m/s
Flame	n_i	1.57	–
	τ_i	*Variable*	s

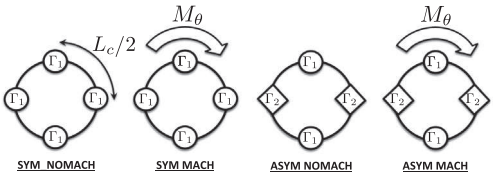

Fig. 5. Configurations leading to symmetry breaking.

3.2. Symmetric case with no mean flow (*Sym NoMach*)

All 4 burners are identical thus matrices $M_i = T_i R_i$ and coupling factors Γ_i are all equal (the subscript i can be omitted here). The dispersion relation (Eq. (16) with $\|\mathcal{S}\| = 0$ and $M_\theta = 0$) has a double root: the mode is degenerate and the expression of the first azimuthal mode frequency (Eq. (18)) reduces to:

$$f = \underbrace{c^0/(2L_c)}_{f^0} - \underbrace{c^0\Gamma^0/(\pi L_c)}_{\delta f} \tag{22}$$

Eq. (22) is compared to results provided by the numerical resolution of Eq. (13) and the 3D acoustic solver in Fig. 6 showing a very good agreement on frequency and growth rate.

In a symmetric configuration, the eigenspace associated to the first azimuthal mode is two-dimensional (the matrix of the system $\prod_{i=4}^{1} M_i$ (Eq. (19)) is the null matrix) so that spinning, standing or mixed mode can occur and have the same growth rate: the mode structure is undetermined. Noiray et al. [5] have shown that non-linearities on the FTF can promote one of these types, a phenomenon which cannot be described by the present linear model.

3.3. Flow symmetry breaking (*Sym Mach*)

Consider now a case with a mean flow (SM effect: $M_\theta \neq 0$) where all burners are identical (i.e. all coupling factors $\mathcal{G}_i$ are equal so that $\|\mathcal{S}\| = 0$). The dispersion relation (Eq. (16) with $\|\mathcal{S}\| = 0$ and $M_\theta \neq 0$) has two distinct solutions so that waves 1 and 2 have different frequencies and growth rates:

$$f_{1,2} = \underbrace{\frac{c^0}{2L_c}}_{f^0} - \underbrace{\frac{c^0\mathcal{G}^{0,\pm M_\theta}}{\pi L_c} \pm \frac{c^0}{2L_c}M_\theta}_{\delta f_1(+),\delta f_2(-)} \tag{23}$$

The mean azimuthal flow modifies the nature of the system: the eigenspace is only one dimensional because the matrix of the system ((Eq. (19) where $\mathcal{S} = 0$ and $M_\theta \neq 0$) does not reduce to the null matrix and (Eq. (20)) gives the nature of the two waves:

- **Wave 1:** $q_4^+ = 0$ and $q_4^- \neq 0$ corresponding to a counter-rotating spinning mode.
- **Wave 2:** $q_4^+ \neq 0$ and $q_4^- = 0$ corresponding to a co-rotating spinning mode.

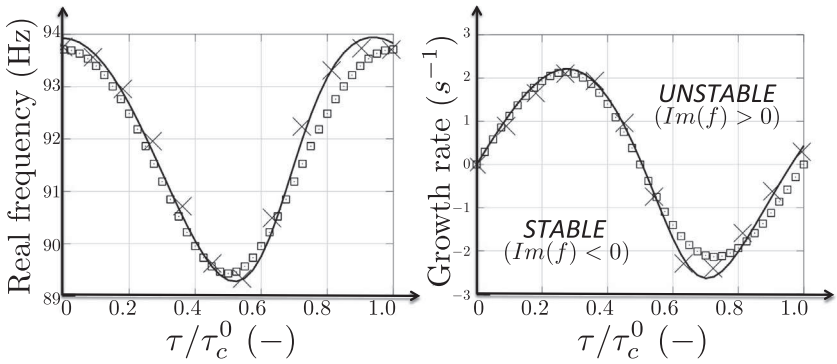

Fig. 6. Frequency (left) and growth rate (right) vs normalized time-delay τ/τ_c^0 (where $\tau_c^0 = 1/f^0$) of the first azimuthal mode in a configuration with $N = 4$ burners. ——: Atacamac (numerical resolution Eq. (13)), □: Atacamac (analytical – Eq. (22)) and ×: 3D acoustic solver

Adding an azimuthal mean flow (M_θ) splits azimuthal modes into two spinning waves with different frequencies and growth rates.

*3.4. GS breaking with no mean flow (**Asym NoMach**)*

The Sym-NoMach case (Section 3.2) is now investigated with two distinct Flame Transfer Functions corresponding to the introduction of two different burner types (i.e. two different coupling parameters Γ_1 and Γ_2) to break symmetry with the pattern 1212 (Fig. 5). The time-delay τ_1 varies from 0 ms to 11 ms while the other time-delay τ_2 is fixed to 2.21 ms.

The dispersion relation (16) gives two different frequencies f_1 and f_2:

$$f_1 = \frac{c^0}{2L_c} - \frac{c^0\Gamma_1^0}{\pi L_c} \text{ and } f_2 = \frac{c^0}{2L_c} - \frac{c^0\Gamma_2^0}{\pi L_c} \tag{24}$$

GS breaking splits the first azimuthal mode in two classes. Mode 1 depends only of Γ_1 and is driven only by the type 1 burners. Mode 2 depends only on Γ_2 and type 2 burners, leading to a constant stability map (Fig. 7) since only τ_1 is varying while τ_2 is fixed.

The splitting strength (Eq. (17)) is non null and controls the degeneracy of the mode ($\|\mathcal{S}\| = 2\|\Gamma_1^0 - \Gamma_2^0\| = \frac{2\pi L_c}{c^0}\|f_2 - f_1\|$) which generalizes the results of Noiray et al. [5] obtained in a simple annular rig not connected to burners.

Due to this splitting, the eigenspace associated to each frequency (f_1 and f_2) is one-dimensional and Eq. (20) gives the nature of the two waves:

- **Wave 1:** $q_4^+/q_4^- = -1$ ($p_4' = 0$) corresponding to a mode locked on the 4^{th} burner (which is of type 2 for the pattern 1212) and imposing a pressure node. This mode is standing and not perturbed by burners of type 2.
- **Wave 2:** $q_4^+/q_4^- = +1$ ($u_4' = 0$) corresponding to a standing mode imposing a velocity node at each burner of type 2 and a pressure node at every burner of type 1: it is perturbed only by burners of type 2 (constant stability map in Fig. 7 since τ_2 is fixed).

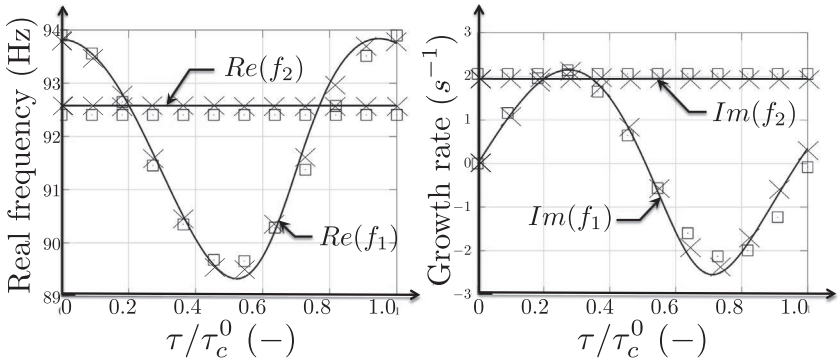

Fig. 7. Frequency (left) and growth rate (right) vs normalized time-delay τ_1/τ_c^0 (where $\tau_c^0 = 1/f^0 \simeq 11\ ms$) while τ_2 is fixed to 2.21 *ms* of the first azimuthal mode in a configuration with $N = 4$ burners. ——: Atacamac (numerical resolution Eq. (13)) and □: Atacamac (analytical – Eq. (24)) and ×: 3D acoustic solver (AVSP).

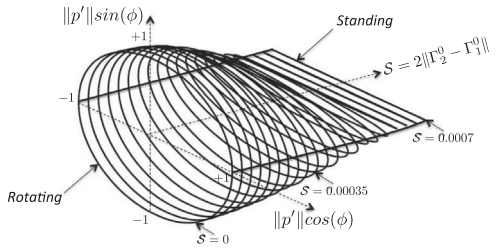

Fig. 8. Structure diagram $(\|p'\|\cos(\phi), \|p'\|\sin(\phi))$ of the Wave 1 vs splitting strength $\|\mathcal{S}\|$. For each splitting strength, the trajectory corresponds to azimuthal positions θ going from 0 to 2π.

A structure diagram [5] $((\|p'\|\cos(\phi), \|p'\|\sin(\phi), \|\mathcal{S}\|)$, Section 3.1) can be constructed (Fig. 8) to highlight the wave nature: if the trajectory at a fixed splitting strength $\|\mathcal{S}\|$ is a circle the wave is spinning ($\phi = \theta$). If the trajectory is a line the wave is standing ($\phi = 0$ or π). Fig. 8 shows the transition of the nature of "Wave 1" from spinning to standing when the splitting strength $\|\mathcal{S}\|$ increases (the time-delay τ_2 is fixed to 2.21 ms and τ_1 can vary). This result is a generalization of the graph "(η_1, η_2, C_{2p})" in [5] for the p^{th} azimuthal mode in the non-linear regime.

3.5. GS and SM breaking (*Asym Mach*)

Using different burner types $\tau_1 = 2.21\ ms$ and $\tau_2 = 4.98\ ms$ leading to a strong splitting term $\|\mathcal{S}\| \simeq 0.145$) and adding a mean azimuthal flow (M_θ can vary) combines GS and SM effects.

The azimuthal mode frequency and structure are given by Eqs. (18) and (20): the mode is mixed and split by both the geometrical (GS, $\|\mathcal{S}\| \neq 0$, Section 3.4) and and flow (SM, $M_\theta \neq 0$, Section 3.3) symmetry breaking (Fig. 9 when $M_\theta = 0.1$).

A configuration where $\tau_1 = 2.21\ ms$ and $\tau_2 = 4.98\ ms$ with a pattern 1212 (corresponding to $\mathcal{S} \simeq 0.145$) is studied by increasing the mean flow from $M_\theta = 0$ *to* 10^{-3}. The structure diagram (Fig. 10, Section 3.1) shows a transition from a standing mode (when the Mach number M_θ is low) to a spinning mode (when M_θ is higher): a small swirl motion (SM) can affect the mode structure even with a strong geometrical symmetry (GS) breaking.

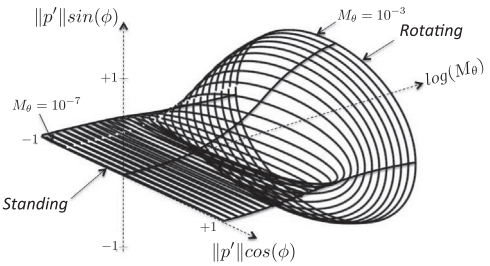

Fig. 10. Structure diagram $(\|p'\|\cos(\phi), \|p'\|\sin(\phi))$ vs Mach number M_θ of the wave associated to the frequency f_1 of a configuration with an initial splitting strength $\mathcal{S} \simeq 0.145$.

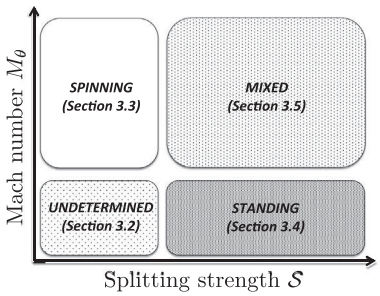

Fig. 11. Effects of geometrical (GS) and flow (SM) symmetry breaking on the mode nature.

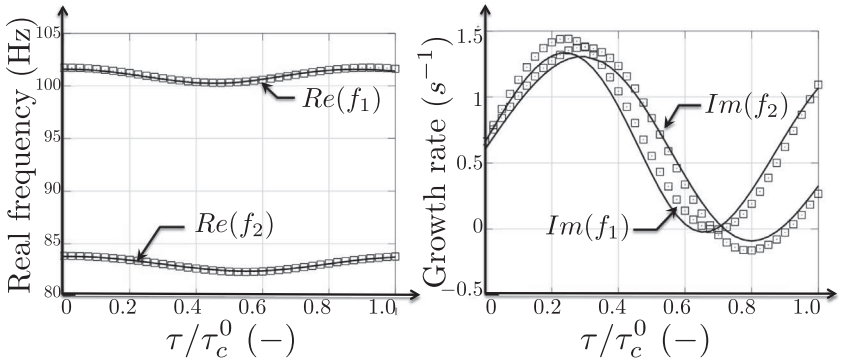

Fig. 9. Frequency (left) and growth rate (right) vs normalized time-delay τ_1/τ_c^0 (where $\tau_c^0 = 1/f^0$) while $\tau_2 = 2.21\ ms$ of the first azimuthal mode in a configuration with $N = 4$ burners and a mean flow $M_\theta = 0.1$. ——: Atacamac (numerical resolution Eq. (13)) and □: Atacamac (analytical – Eq. (18)).

4. Conclusion

This paper presents an analytical approach to study two mechanisms controlling azimuthal modes frequency and nature (spinning, standing or mixed) in annular combustors containing 4 burners: (1) the circumferential variation of burner characteristics and (2) the existence of a mean azimuthal flow. The ATACAMAC methodology [17] is extended to solve the linearized acoustic equations with a steady and uniform azimuthal mean flow in the annular chamber. It provides an analytical implicit dispersion relation for the frequency f which can be solved numerically. An analytical resolution is possible in specific situations where the annular chamber is weakly coupled to the burners. Results show that symmetry breaking, either by modifying burner characteristics or with a swirl motion, splits the azimuthal mode into two waves which can have different but close frequencies and structures. Results are summarized in Fig. 11 showing the nature of the two components of the azimuthal mode as a function of mean Mach number M_θ and splitting strength $\mathcal{S}$. However, as for non-linear theories [5,13] or acoustic simulations, only the nature of these two components A and B can be determined but their ratio A/B fixing the final mode structure remains unknown and would requires high fidelity simulations or the complete resolution of the mode dynamics (where the critical issue would be the determination of the initial condition). Nevertheless, this theory could be validated by the extraction of the splitting frequency as well as the nature of the two components from LES or experiments. No experimental validation has been performed yet but annular systems available at Cambridge [9] or EM2C [8] would be excellent setups to verify the validity of this model which was derived here for 4 burners but is expected to be also valid for real chambers with more burners.

References

[1] W. Krebs, P. Flohr, B. Prade, S. Hoffmann, *Combust. Sci. Tech.* 174 (2002) 99–128.
[2] T. Lieuwen, V. Yang, *AIAA* (2005).
[3] C. Pankiewitz, T. Sattelmayer, *ASME J. Eng. Gas Turbines Power* 125 (3) (2003) 677–685.
[4] T. Poinsot, D. Veynante, Theoretical and Numerical Combustion, (third ed.) (www.cerfacs.fr/elearning), 2011.
[5] N. Noiray, M. Bothien, B. Schuermans, *Combust. Theor. Model.* (2011) 585–606.
[6] G. Staffelbach, L. Gicquel, G. Boudier, T. Poinsot, in: Proc. Combust. Inst., 32, 2009, pp. 2909–2916,.
[7] P. Wolf, G. Staffelbach, L. Gicquel, J. Muller, T. Poinsot, *Combust. Flame* 159 (2012) 3398–3413.
[8] J.-F. Bourgouin, D. Durox, J. Moeck, T. Schuller, S. Candel, in: ASME Turbo Expo, GT2013-95010, 2013.
[9] N. Worth, J. Dawson, in: Proc. Combust. Inst., 34, 2013, pp. 3127–3134.
[10] N. Noiray, B. Schuermans, in: Proceedings of the Royal Society A: Mathematical, Physical and Engineering Sciences, 2012-0535, 2012.
[11] B. Schuermans, C. Paschereit, P. Monkewitz, in: 44th AIAA Aerospace Sciences Meeeting and Exhibit, 2006-0549, 2006.
[12] C. Sensiau, F. Nicoud, T. Poinsot, *Int. J. Aeroacoust.* 8 (1) (2009) 57–68.
[13] G. Ghirardo, M. Juniper, in: Proceedings of the Royal Society A, 2013-0232, 2013.
[14] A.S. Morgans, S.R. Stow, *Combust. Flame* 150 (4) (2007) 380–399.
[15] J. Parmentier, P. Salas, P. Wolf, G. Staffelbach, F. Nicoud, T. Poinsot, *Combust. Flame* 159 (2012) 2374–2387.
[16] S. Evesque, W. Polifke, C. Pankiewitz, in: 9th AIAA/CEAS Aeroacoustics Conference, volume AIAA paper 2003-3182, 2003.
[17] M. Bauerheim, J. Parmentier, P. Salas, F. Nicoud, T. Poinsot, *Combust. Flame* 161 (2014) 1374–1389.
[18] J. Moeck, M. Paul, C. Paschereit, in: ASME Turbo Expo, GT2010-23577, 2010.
[19] N. Worth, J. Dawson, *Combust. Flame* 160 (11) (2013) 2476–2489.
[20] J. O'Connor, T. Lieuwen, *Phys. Fluids* 24 (2012) 075107.
[21] J. Blimbaum, M. Zanchetta, T. Akin, et al., *Int. J. Spray Combust. Dyn.* 4 (4) (2012) 275–298.
[22] S.R. Stow, A.P. Dowling, in: ASME Paper 2003-GT-38168, Atlanta, Georgia, USA, 2003.
[23] A.P. Dowling, *J. Sound Vib.* 180 (4) (1995) 557–581.
[24] S.R. Stow, A.P. Dowling, in: ASME Paper, 2001-GT-0037, New Orleans, Louisiana, 2001.
[25] E. Motheau, F. Nicoud, T. Poinsot, Proceeding of ASME Turbo Expo GT2012-68852 2012.
[26] P. Palies, Dynamique et instabilités de combustion de flammes swirlées, PhD thesis, Ecole Centrale Paris, 2010.
[27] T. Schuller, D. Durox, P. Palies, S. Candel, *Combust. Flame* 159 (2012) 1921–1931.
[28] W. Krebs, G. Walz, P. Flohr, S. Hoffmann, in: ASME Turbo Expo, 2001-GT-42, 2001.
[29] F. Nicoud, L. Benoit, C. Sensiau, T. Poinsot, *AIAA J.* 45 (2007) 426–441.